An Efficient GFET Structure

Giovanni Nastasi and Vittorio Romano

***Abstract*— A graphene FET (GFET), where the active area is made of monolayer large-area graphene, is simulated including a full 2-D Poisson equation and a drift-diffusion model with mobilities deduced by a direct numerical solution of the semiclassical Boltzmann equations for charge transport by a suitable discontinuous Galerkin approach. The critical issue in a GFET is the difficulty of fixing the OFF state which requires an accurate calibration of the gate voltages. In this article, we propose and simulate a GFET structure which has well-behaved characteristic curves similar to those of conventional (with gap) semiconductor materials. The introduced device has a clear off region and can be the prototype of devices suited for postsilicon nanoscale electron technology. The specific geometry overcomes the problems of triggering the minority charge current and gives a viable way for the design of electron devices based on large area monolayer graphene as a substitute of standard semiconductors in the active area. The good FET behavior of the current versus the gate voltage makes the simulated device very promising and a challenging case for experimentalists, even if it is crucial to better understand the resistance effect of charge carriers at the contact-graphene region.**

***Index Terms*— Discontinuous Galerkin (DG) method, drift-diffusion, graphene FET (GFET), graphene, mobility model.**

I. Introduction

THE MOSFET is the backbone of the modern integrated circuits. In the case, the active area is made of traditional materials, for example, silicon or gallium arsenide, a lot of analysis and simulations have been performed in order to optimize the design. Lately, a great attention has been devoted to graphene on account of its peculiar features, and in particular, from the point of view of nanoelectronics, for the high electrical conductivity. It is highly tempting to try to replace the traditional semiconductors with graphene in the active area of electron devices like the MOSFETs [1] even if many aspects about the actual performance in real applications remain unclear.

Manuscript received March 25, 2021; revised June 3, 2021; accepted July 6, 2021. Date of publication July 26, 2021; date of current version August 23, 2021. This work was supported by the Università degli Studi di Catania, Piano della Ricerca 2020/2022 Linea di intervento 2 "QICT." The work of Giovanni Nastasi was supported by the National Group of Mathematical Physics (GNFM-INdAM) Progetti Giovani GNFM 2020. The review of this article was arranged by Editor F. Schwierz. *(Corresponding author: Vittorio Romano.)*

The authors are with the Department of Mathematics and Computer Science, University of Catania, 95125 Catania, Italy (e-mail: g.nastasi@unict.it; romano@dmi.unict.it).

Color versions of one or more figures in this article are available at https://doi.org/10.1109/TED.2021.3096492.

Digital Object Identifier 10.1109/TED.2021.3096492

Scaling theory predicts that an FET with a thin barrier and a thin gate-controlled region will be robust against short-channel effects down to very short gate lengths. The possibility of having channels that are just one atomic layer thick is perhaps the most attractive feature of graphene for its use in transistors. Main drawbacks of a large-area single monolayer graphene are the zero gap and, for graphene on substrate, the degradation of the mobility. Therefore, accurate simulations are warranted for the setup of a viable graphene FET (GFET).

The standard mathematical model is given by the drift-diffusion-Poisson system. Usually, the GFETs are investigated by adopting reduced 1-D models of the Poisson equation with some averaging procedure [2]–[4]. Here, a full 2-D simulation is presented.

A crucial point is the determination of the mobilities entering the drift-diffusion equations. A rather popular model is that proposed in [5]. Here, a different approach is adopted. Thanks to the discontinuous Galerkin (DG) scheme developed in [6]–[8], we have performed, for graphene on a substrate, an extensive numerical simulation based on the semiclassical Boltzmann equations, including electron–phonon and electron-impurity scatterings along with the scattering with remote phonons of the substrate. Both intra and inter-band scatterings have been taken into account. For other simulation approaches the interested reader is referred to [9] and [10]. Quantum effects have been also introduced in [11]–[13]. An alternative approach could be resorting to hydrodynamical models (see [14]–[16]).

From the numerical solutions of the semiclassical Boltzmann equation a model for the mobility functions has been deduced, similar to what already done in [17] and [18] in the case of suspended monolayer graphene.

In this article, we propose a slightly different geometry of GFET which leads to a clear and sizable off region, avoiding the problem of triggering the minority charge carriers and producing characteristic curves which seem very promising for the use of large-area graphene in electron devices.

The plan of this article is as follows. In Section II, the structure of the proposed device is presented along with the mathematical model. In Section III, the mobilities are sketched, and in Section IV the numerical simulations of the proposed GFET are shown and compared with devices having graphene as active area and a standard geometry already known in the literature.

II. Device Structure and Mathematical Model

We propose the device with the geometry depicted in Fig. 1. The active zone is made of a single layer of graphene which is

between two strips of insulator, both of them being SiO_2. The source and drain contacts are directly attached to the graphene. The two gate contacts (up and down) are attached to the oxide. The choice of the type of oxide is not crucial at this stage. We have considered SiO_2 as an example but other oxides such as h-BN can be also easily considered. Instead it is crucial to put the source and drain contacts along all the lateral edges for a better control of the electrostatic potential as will be clear from the simulations. In the direction orthogonal to the section the device is considered infinitely long.

We solve a 2-D Poisson equation, assuming that the charge is distributed in the volume between the two strips of oxide. The distance t_{gr} between the two layers of oxide has been investigated by direct measurements. Note that it is greater than the simple graphene thickness because also the double interatomic oxide/graphene distance must be included. A monolayer of graphene is about 0.335-nm thick (0.35 nm when obtained by chemical vapor decomposition) while values between 0.4 and 1.7 nm are reported for t_{gr} in [19] in the case of a single graphene/oxide interface by using atomic force microscopy. In [20], according to [21], a nominal value of 0.4 nm is assumed for taking into account the graphene/oxide and the graphene/tip interaction. In [22] for graphene over Cu(111) an interstitial distance of 0.321 nm is adopted. Upon these considerations, in our simulation, we set $t_{gr} = 1$ nm as an indicative value for a double graphene/oxide interface.

In order to simulate the current flowing in the channel we adopt the 1-D bipolar stationary drift-diffusion model

$$\frac{\partial J_n}{\partial x} = eR, \quad \frac{\partial J_p}{\partial x} = -eR \tag{1}$$

e being the (positive) elementary charge, coupled to the 2-D Poisson equation for the electrostatic potential in the whole section. The electron and hole current densities are given by (see [23])

$$J_n = \mu_n n \frac{\partial \varepsilon_F^{(n)}}{\partial x}, \quad J_p = \mu_p p \frac{\partial \varepsilon_F^{(p)}}{\partial x} \tag{2}$$

where n and p, $\varepsilon_F^{(n)}$ and $\varepsilon_F^{(p)}$, μ_n, and μ_p are the densities, quasi-Fermi energies and mobilities of electrons and holes, respectively. R denotes the generation-recombination term. The expression of R is still a matter of debate. A typical behavior of the total generation-recombination term versus time, obtained with the DG method [6]–[8], can be found in [24]. However, from these simulations a dependence on the space variable is not easy to extrapolate. Therefore, we resort to the expression suggested in [25] by analogy with standard semiconductors

$$R = \frac{np - n_e p_e}{\tau\left(n + p + 2\sqrt{n_e p_e}\right)} \tag{3}$$

where n_e and p_e are the equilibrium electron and hole densities and τ is the generation-recombination relaxation time. Indeed, in order to describe tunneling effects, in [25] an additional contribution has been included which contains several parameters to be determined by experiments. However, due to the zero gap in the energy band, the inter-band scattering induced by the electron-phonon scattering is much more effective than tunneling mechanism. For such a reason only the Shockley–Read-Hall-type term is retained in R.

The electron and hole densities, $n(x)$ and $p(x)$ respectively, are evaluated as

$$n(x) = \frac{g_s g_v}{(2\pi)^2} \int_{\mathbb{R}^2} f_{FD}(\mathbf{k}, \varepsilon_F^{(n)})\, d\mathbf{k}, \quad x \in [x_1, x_4]$$
$$p(x) = \frac{g_s g_v}{(2\pi)^2} \int_{\mathbb{R}^2} f_{FD}(\mathbf{k}, -\varepsilon_F^{(p)})\, d\mathbf{k}, \quad x \in [x_1, x_4]$$

with $g_s = 2$ and $g_v = 2$ the spin and valley degeneracy. f_{FD} indicates the Fermi–Dirac distribution

$$f_{FD}(\mathbf{k}, \varepsilon_F) = \left[1 + \exp\left(\frac{(\varepsilon(\mathbf{k}) - \varepsilon_D) - (\varepsilon_F - \varepsilon_D)}{k_B T}\right)\right]^{-1}$$

where $\varepsilon_D = -e\phi(x, y_{gr})$ is the Dirac energy and $\phi(x, y)$ is the electrical potential, here evaluated on $y = y_{gr}$, y_{gr} being the average y-coordinate of the graphene sheet (see Fig. 1). ε_F denotes the Fermi level (in pristine graphene $\varepsilon_F = \varepsilon_D$), $\varepsilon(\mathbf{k}) - \varepsilon_D = \hbar v_F |\mathbf{k}|$ represents the graphene dispersion relation (strictly valid around the Dirac points), which is the same for electrons and holes (see [26]–[28]), $\hbar$ is the reduced Planck constant, v_F the Fermi velocity, k_B Boltzmann's constant, T the lattice temperature, kept at 300 K (room temperature). The crystal momentum of electrons and holes is assumed to vary over $\mathbb{R}^2$.

By observing that $d\mathbf{k} = ((\varepsilon - \varepsilon_D) d(\varepsilon - \varepsilon_D)\, d\varphi/(\hbar v_F)^2)$, with φ azimuthal angle of $\mathbf{k}$, the previous relations can be written in terms of the Fermi integrals of order k

$$\mathcal{F}_k(\eta) = \frac{1}{\Gamma(k+1)} \int_0^{+\infty} \frac{\chi^k}{1 + e^{\chi - \eta}}\, d\chi$$

with $\Gamma(x)$ Euler gamma function, obtaining

$$n(x) = \frac{2}{\pi}\left(\frac{k_B T}{\hbar v_F}\right)^2 \mathcal{F}_1\left(\frac{\varepsilon_F^{(n)} - \varepsilon_D}{k_B T}\right) \tag{4}$$

$$p(x) = \frac{2}{\pi}\left(\frac{k_B T}{\hbar v_F}\right)^2 \mathcal{F}_1\left(-\frac{\varepsilon_F^{(p)} - \varepsilon_D}{k_B T}\right). \tag{5}$$

System (1) is set in the interval $[x_1, x_4]$ and is augmented with Dirichlet boundary conditions for electron and hole densities as will be explained in the following.

A special attention is required by the initial carrier density profiles that have to be determined compatibly with the electric potential, leading to a nonlinear Poisson equation as discussed in the following.

The electric potential solves the 2-D Poisson equation

$$\nabla \cdot (\epsilon \nabla \phi) = h(x, y) \tag{6}$$

where $h(x, y) = e(n(x) - p(x) - n_i)/t_{gr}$ if $(x, y) \in [x_1, x_4] \times [y_2, y_3]$ and $h(x, y) = 0$ otherwise. ϵ is given by ϵ_{gr} if $y \in [y_2, y_3]$ and ϵ_{ox} otherwise. Here, $\epsilon_{gr} = 3.3\,\epsilon_0$ and $\epsilon_{ox} = 3.6\,\epsilon_0$ are the dielectric constants of the graphene and oxide (SiO_2) respectively, ϵ_0 being the dielectric constant in the vacuum. n_i is the areal density of the impurity charges at the graphene/oxide interface. We set $n_i = 2.5 \cdot 10^3\ \mu\mathrm{m}^{-2}$. The charge in the graphene layer is considered as distributed in the volume enclosed by the parallelepiped of base the area of

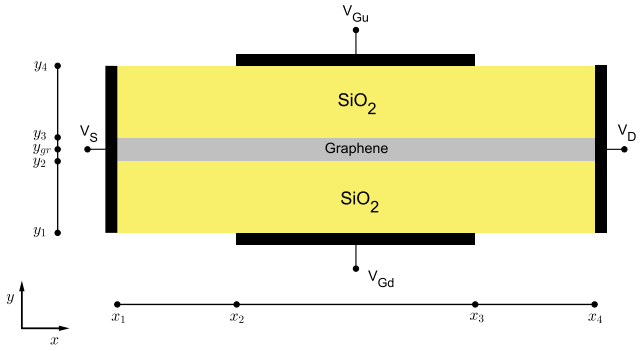

Fig. 1. Schematic of the GFET investigated in this article.

the graphene and height $t_{\rm gr}$. Recall that n and p are areal densities. Dirichlet conditions are imposed at the contacts and homogeneous Neumann conditions on the external oxide edges.

A major issue is to model the source and drain regions where metal and graphene touch. We assume that source and drain are thermal bath reservoirs where charges obey a Fermi-Dirac distribution. The injection of charges is determined by the difference of the work functions between contact and graphene. Of course, it depends on the specific material the contacts are made of. Copper is considered as one of the best materials on which to deposit graphene by chemical vapor deposition technique. Moreover, the interaction between Cu and graphene is the weakest among metals. Density function theory (DFT) calculations [22] predict a shift $\Delta\varepsilon_F = 0.275$ eV of the Fermi energy with respect to the energy at the Dirac point at the copper/graphene junction in the case of Cu(111), creating an induced n-doping. This is within the experimentally observed range between 0.20 eV [29] and 0.30 eV [30] of the shift of the Fermi energy. In the sequel, we will use the indicative value $\Delta\varepsilon_F = 0.25$ eV.

An additional effect to take into account is the resistance at the contact due to the fact that the quantum states in graphene are not all available (see [31]). From a macroscopic point of view, we model this fact by reducing the injected charges by multiplying the Fermi energy shift $\Delta\varepsilon_F$ by a factor $0 < \alpha \leq 1$.

As summary, the following boundary conditions are imposed upon the system (1) and (6). The quasi Fermi potentials satisfy

$$lcl\varepsilon_F^{(n)}(x_1) - \varepsilon_D(x_1) = \varepsilon_F^{(p)}(x_1) - \varepsilon_D(x_1) = \alpha\Delta\varepsilon_F \quad (7)$$

$$\varepsilon_F^{(n)}(x_4) - \varepsilon_D(x_4) = \varepsilon_F^{(p)}(x_4) - \varepsilon_D(x_4) = \alpha\Delta\varepsilon_F \quad (8)$$

while for the electric potential

$$\begin{aligned} \phi &= 0 \quad \text{at} \quad y \in [y_1, y_4],\ x = x_1 \\ \phi &= V_b \quad \text{at} \quad y \in [y_1, y_4],\ x = x_4 \\ \phi &= V_{G_d} \quad \text{at} \quad y = y_1,\ x \in [x_2, x_3] \\ \phi &= V_{G_u} \quad \text{at} \quad y = y_4,\ x \in [x_2, x_3] \\ \nabla_\nu \phi &= 0 \quad \text{at the remaining part of} \\ &\qquad \text{the boundary.} \end{aligned} \quad (9)$$

V_b is the bias voltage, V_{G_u} is the upper gate–source potential, V_{G_d} is the down gate–source potential. V_{G_u} and V_{G_d} include the (subtracted) flat-band voltages. We have denoted by ∇_ν the external normal derivative.

Regarding the densities from the previous conditions it follows that:

$$n(x_1) = n(x_4) = \frac{2}{\pi}\left(\frac{k_B T}{\hbar v_F}\right)^2 \mathcal{F}_1\left(\frac{\alpha\Delta\varepsilon_F}{k_B T}\right) \quad (10)$$

$$p(x_1) = p(x_4) = \frac{2}{\pi}\left(\frac{k_B T}{\hbar v_F}\right)^2 \mathcal{F}_1\left(-\frac{\alpha\Delta\varepsilon_F}{k_B T}\right). \quad (11)$$

III. Mobility Model

We adopt the mobilities deduced in [24] from a direct numerical simulation of the transport equations by using a DG scheme (the interested reader is referred to [6] and [8] for the details). The behavior is the same for holes on account of the symmetry between the hole and electron distributions.

The low field mobility has the expression

$$\mu_0(n) = \tilde{\mu}_1 - \tilde{\mu}_0 \frac{\exp\left(-\frac{(\log(n/n_{\rm ref})-m)^2}{2\sigma^2}\right)}{\sqrt{2\pi}\sigma n/n_{\rm ref}} \times\left(a\left(\frac{n}{n_{\rm ref}}\right)^2 + b\frac{n}{n_{\rm ref}} + c\right)$$

where the fitting parameters have been estimated by the least squares method as follows $\tilde{\mu}_0 = 0.2978$ μm^2/V ps, $\tilde{\mu}_1 = 4.223$ μm^2/V ps, $n_{\rm ref} = 376.9$ μm^{-2}, $m = -0.2838$, $\sigma = 2.216$, $a = 4.820$, $b = 68.34$ and $c = 2.372$.

The complete mobility model is given by (see also [17], [18])

$$\mu(E, n) = \frac{\mu_0(n) + \tilde{\mu}\left(\frac{E}{E_{\rm ref}}\right)^{\beta_1}}{1 + \left(\frac{E}{E_{\rm ref}}\right)^{\beta_2} + \gamma\left(\frac{E}{E_{\rm ref}}\right)^{\beta_3}} \quad (12)$$

where E is the modulus of longitudinal component of the electric field while $E_{\rm ref}$, $\tilde{\mu}$, β_1, β_2, β_3, and γ are fitting parameters.

We have calculated the coefficients $E_{\rm ref}$, β_1, β_2, β_3, γ and $\tilde{\mu}$ by means of least square method for several value of the electron density n_i, obtaining the data reported in Table I. The values of the density correspond to the Fermi energies 0.1, 0.2, 0.3, 0.4, and 0.5 eV. In each interval $[n_i, n_{i+1}]$ a third degree polynomial interpolation has been adopted for the parameters $E_{\rm ref}$, β_1, β_2, β_3, γ, and $\tilde{\mu}$ [24].

IV. Numerical Simulations

The GFET of Fig. 1 has been intensively simulated. We have set the length 100 nm, the width of the lower and upper oxide (SiO_2) 10 nm. The gate contacts are long 50 nm. The lateral (source and drain) contacts are long 21 nm. The two gate potentials are set equal in the simulated cases. We considered a mesh of 40 grid points along the x-direction and 23 grid points along the y-direction. In the graphene layer a single row of 40 nodes has been employed. If not stated otherwise, we set $\alpha = 1$ and $\tau = 1$ ps.

In order to get the numerical solutions, a strategy similar to that used in [32] has been adopted, even if we remark

TABLE I

HIGH FIELD MOBILITY PARAMETERS. n_i IS EXPRESSED IN μm^{-2}, THE REFERENCE FIELD E_{REF} IS EXPRESSED IN V/μm, THE MOBILITY $\tilde{\mu}$ IS EXPRESSED IN μm^2/V ps. THE PARAMETERS β_i AND γ ARE DIMENSIONLESS

n_i	E_{ref}	β_1	β_2	β_3	γ	$\tilde{\mu}$
4471	0.05265	1.034	2.135	1.059	14.53	12.78
15500	0.02126	0.4615	1.584	0.4276	21.77	33.3
33877	0.1096	1.344	2.52	1.457	4.595	6.579
59588	0.1776	2.304	3.099	1.335	1.395	1.251
92644	0.05047	1.988	2.661	1.109	0.8816	1.915

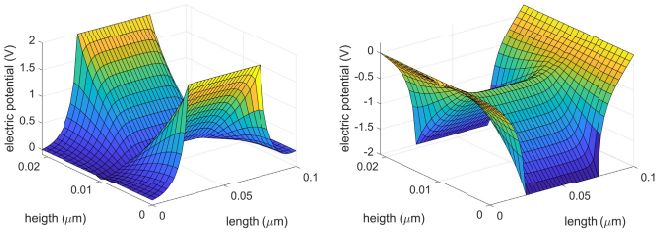

Fig. 2. Electrostatic potential with $V_b = 0.2$ V. Left: case of $V_G = 2$ V (ON state). Right: case of $V_G = -2$ V (OFF state).

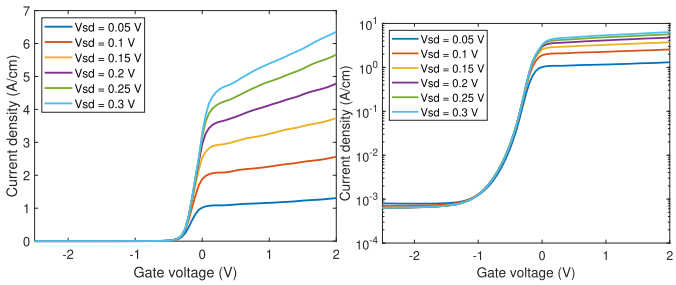

Fig. 3. Total current versus gate voltage for the GFET of Fig. 1 obtained with model (1) and (6) at fixed bias in linear scale (left) and semilogarithmic scale (right).

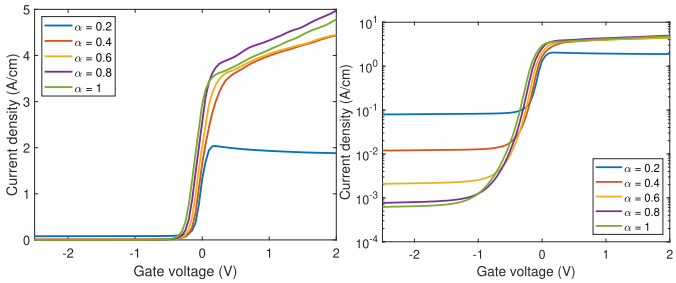

Fig. 4. Total current versus gate voltage for the GFET of Fig. 1 at fixed bias of 0.2 V and for several values of α in linear scale (left) and semilogarithmic scale (right).

that in this article two different quasi Fermi potentials are used and the Poisson equation is solved in the whole device. Starting from an initial guess for the electron and hole quasi Fermi potentials and for the electrostatic potential, an initial guess for the electron and hole densities is deduced. Inserting those into the Poisson equation an approximation of the electrostatic potential in the whole device is obtained by a finite difference numerical scheme. Then (1) are solved by finite differences and a new approximation of the quasi Fermi potential is computed. Iterating we get the stationary solution to system (1) and (6). In order to improve the convergence, Pulay's method has been employed as in [32]. The difference between two iterations is measured as the relative variation of the current $e_n = (\|J_n^{k+1} - J_n^k\|)/(\|J_n^{k+1}\|)$ and $e_p = (\|J_p^{k+1} - J_p^k\|)/(\|J_p^{k+1}\|)$, where J_n^k and J_p^k are the electron and hole currents at the kth iteration. As stopping criterion e_n and e_p less than 10^{-4} has been required. Here, $\|\cdot\|$ denotes the supremum norm.

A typical shape of obtained 2-D electrostatic potential is reported in Fig. 2 while the characteristic curves are shown in Fig. 3. It is evident that an acceptable field effect transistor is obtained. By decreasing the gate voltage the current settles at a very low value. The plot in logarithmic scale shows a current-ON/current-OFF ratio of five orders of magnitude. The minority charges are only slightly activated, the charge transport is bipolar but the inversion gate voltage observed with other geometries [1] is practically not present. The main reason for such an effect is the peculiar position and breadth of the source and drain contacts which create an electrostatic potential such that the electrochemical energy is always of constant sign. However, we observe that this effect depends on the value of the contact resistance, as shown in Fig. 4 where the current versus the gate voltage is plotted for several values of α. Smaller α's lead to a smaller ratio current-OFF/current-ON. If $\alpha = 0.2$ such a ratio is only about one order of magnitude against the about four orders of magnitude if $\alpha = 1$. This prompts to better investigate the actual charge density in the hybrid region contact-graphene, the crucial parameter being $\alpha\Delta\varepsilon_F$.

For comparison, in Fig. 5 the results obtained with the model including a single Fermi level are also shown. The behavior is similar but there are nonnegligible quantitative differences in the currents. This indicates that the use of a single Fermi level is not accurate enough.

Devising a working structure has required a full 2-D numerical solution of the Poisson equation. The common use of lumped 1-D models for the electrostatic potential has the drawback of hiding the effects related to the source and drain contact position and breadth.

The simulations have been also performed adopting the mobility model in [5]. The results are qualitatively in good agreement with those obtained by using the mobility model of Section III. Therefore, we are rather confident that the efficient FET performance of the proposed device is not an artifact related to the adopted specific mobility model but a general feature stemming from the chosen geometry. The proposed device overcomes the drawback related to the zero gap in pristine large area graphene and represents a viable prototype for the design of efficient GFETs.

We have also performed the simulations with higher values of τ, 10 and 100 ps. The qualitative behavior is practically the same but with an improved current-ON/current-OFF ratio and this suggests that the generation-recombination term does not affect the good FET performance.

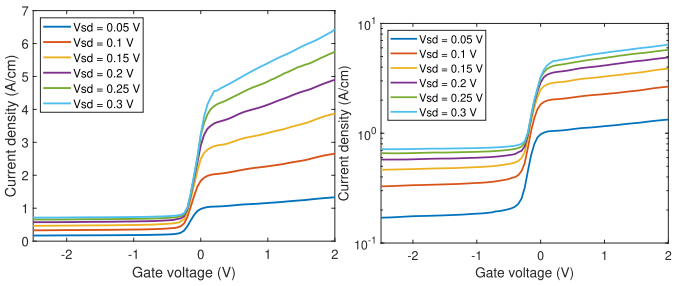

Fig. 5. Total current versus gate voltage for the GFET of Fig. 1 for the model with a single Fermi level at fixed bias in linear scale (left) and semilogarithmic scale (right).

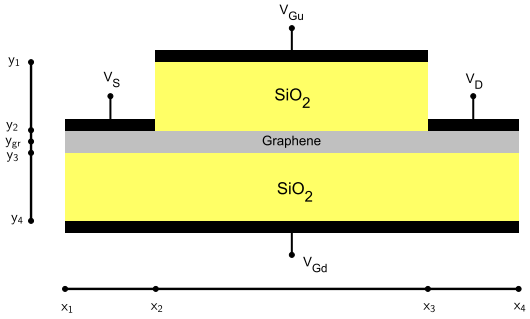

Fig. 6. Schematic of a standard GFET considered in [24]. In the direction orthogonal to the section the device is considered long enough so that the boundary effect can be neglected.

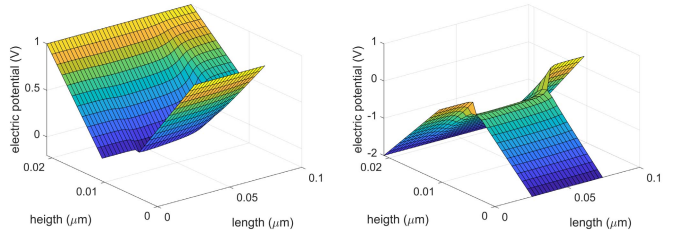

Fig. 7. Electrostatic potential with $V_b = 0.4$ V for the device of Fig. 6. On top the case of $V_G = 1$ V. At the bottom the case of $V_G = -2$ V.

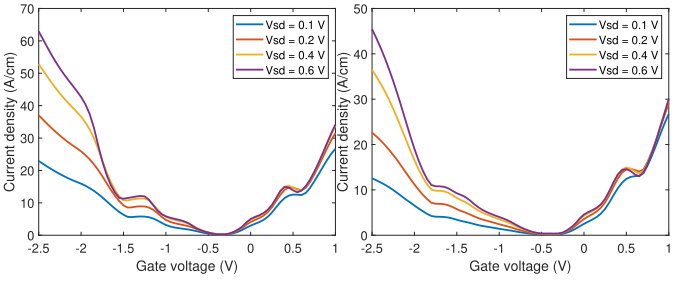

Fig. 8. Total current versus gate voltage for the GFET of Fig. 6 in the case with two Fermi levels (left) and in the case with one Fermi level (right) at fixed bias.

To better understand the reached improvement, we include also the results for a standard GFET, already investigated in the literature, depicted in Fig. 6. We have obtained the characteristic curves with the same approach described in the previous section (the interested reader is referred to [24] for the details). The potential is plotted in Fig. 7, the relative characteristics are reported in Fig. 8 which shows that below a

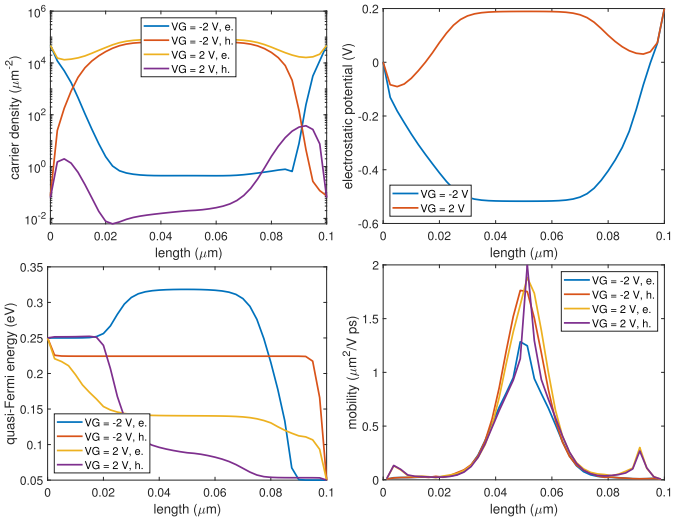

Fig. 9. Carrier densities (top-left), electrostatic potential (top-right), quasi-Fermi energy (bottom-left) and mobility (bottom-right) relative to the device of Fig. 1 obtained by the model with two Fermi levels in the case $V_b = 0.2$ V and $V_G = -2$ and 2 V.

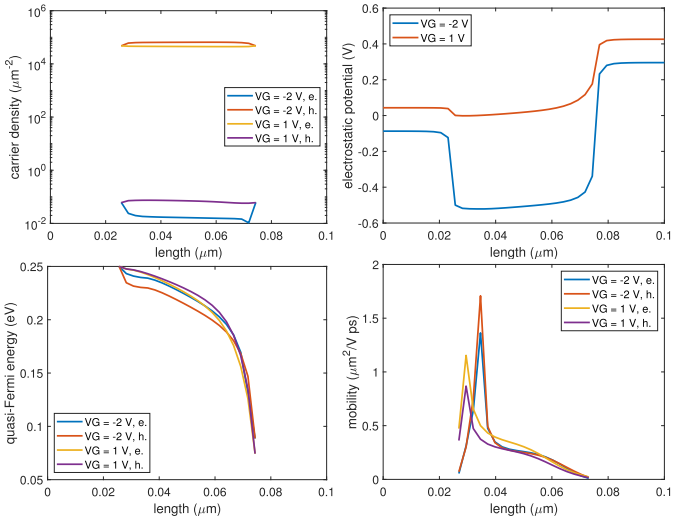

Fig. 10. Carrier densities (top-left), electrostatic potential (top-right), quasi-Fermi energy (bottom-left) and mobility (bottom-right) relative to the device of Fig. 6 obtained by the model with two Fermi levels in the case $V_b = 0.4$ V and $V_G = -2$ and 1 V.

threshold voltage the minority charges activate and this limits the off region to a restricted range of gate voltages. The simpler model with a single Fermi level has been adopted as well for the sake of completeness. In this case, the model with a single Fermi level seems to be closer to the full two Fermi levels model than the previous device (see Fig. 5).

Since for both devices the same model and numerical scheme has been adopted, the different performance can only be ascribed to the different geometry. In order to better explain that, in Fig. 9 we report the carrier densities, the electrostatic potential, the quasi-Fermi energy and the mobility in the graphene channel of the device of Fig. 1 in a ON state case and OFF state one. In Fig. 10 the same quantities are reported for the device of Fig. 6. The main peculiarity is that in the device of Fig. 1 we have a sizeable difference between the electron and hole densities while in the device of Fig. 6 these densities are much closer. This is a consequence of the resulting Fermi

levels which in turn depend on the specific shape of the electrostatic potential. It seems that the lumped 1-D solutions of the Poisson equation misses relevant features correlated with the geometry of the device.

V. Conclusion

A peculiar GFET has been studied by a full numerical solution of a drift-diffusion-Poisson model with mobilities obtained from the direct solution of the Boltzmann equations for charge transport in graphene. The specific geometry overcomes the problem of triggering the minority charge current and gives a viable way for the design of electron devices based on large area monolayer graphene as substitute of standard semiconductors in the active area. The good FET behavior of the current versus the gate voltage makes the simulated device very promising and a challenging case for experimentalists, even if it is crucial to better understand the resistance effect of charge carriers at the contact-graphene region.

We remark that the diriment point is the way the electrostatic is determined by the choice of the geometry, in particular the position of the contacts. The full 2-D numerical solution of the Poisson equation has played a crucial role for the simulation of the current in the proposed device and its optimization.

References

[1] F. Schwierz, "Graphene transistors," *Nature Nanotechnol.*, vol. 5, no. 7, pp. 487–496, May 2010, doi: 10.1038/nnano.2010.89.

[2] D. Jiménez and O. Moldovan, "Explicit drain-current model of graphene field-effect transistors targeting analog and radio-frequency applications," *IEEE Trans. Electron Devices*, vol. 58, no. 11, pp. 4049–4052, Nov. 2011, doi: 10.1109/TED.2011.2163517.

[3] A. K. Upadhyay, A. K. Kushwaha, and S. K. Vishvakarma, "A unified scalable quasi-ballistic transport model of GFET for circuit simulations," *IEEE Trans. Electron Devices*, vol. 65, no. 2, pp. 739–746, Feb. 2018, doi: 10.1109/TED.2017.2782658.

[4] I. Meric, M. Y. Han, A. F. Young, B. Ozyilmaz, P. Kim, and K. L. Shepard, "Current saturation in zero-bandgap, top-gated graphene field-effect transistors," *Nature Nanotechnol.*, vol. 3, no. 11, pp. 654–659, 2008, doi: 10.1038/nnano.2008.268.

[5] V. E. Dorgan, M.-H. Bae, and E. Pop, "Mobility and saturation velocity in graphene on SiO_2," *Appl. Phys. Lett.*, vol. 97, no. 8, Aug. 2010, Art. no. 082112, doi: 10.1063/1.3483130.

[6] M. Coco, A. Majorana, and V. Romano, "Cross validation of discontinuous Galerkin method and Monte Carlo simulations of charge transport in graphene on substrate," *Ricerche Matematica*, vol. 66, no. 1, pp. 201–220, Jun. 2017, doi: 10.1007/s11587-016-0298-4.

[7] M. Coco, A. Majorana, G. Nastasi, and V. Romano, "High-field mobility in graphene on substrate with a proper inclusion of the Pauli exclusion principle," *Atti Della Accademia Peloritana Pericolanti-Classe Scienze Fisiche, Matematiche Naturali*, vol. 96, no. S1, May 2019, Art. no. A6, doi: 10.1478/AAPP.97S1A6.

[8] A. Majorana, G. Nastasi, and V. Romano, "Simulation of bipolar charge transport in graphene by using a discontinuous Galerkin method," *Commun. Comput. Phys.*, vol. 26, no. 1, pp. 114–134, Feb. 2019, doi: 10.4208/cicp.OA-2018-0052.

[9] P. Lichtenberger, O. Morandi, and F. Schürrer, "High-field transport and optical phonon scattering in graphene," *Phys. Rev. B, Condens. Matter*, vol. 84, no. 4, Jul. 2011, Art. no. 045406, doi: 10.1103/PhysRevB.84.045406.

[10] O. Muscato and W. Wagner, "A class of stochastic algorithms for the Wigner equation," *SIAM J. Sci. Comput.*, vol. 38, no. 3, pp. A1483–A1507, Jan. 2016, doi: 10.1137/16M105798X.

[11] L. Barletti, "Hydrodynamic equations for electrons in graphene obtained from the maximum entropy principle," *J. Math. Phys.*, vol. 55, no. 8, Aug. 2014, Art. no. 083303, doi: 10.1063/1.4886698.

[12] O. Morandi and F. Schürrer, "Wigner model for quantum transport in graphene," *J. Phys. A, Math. Theor.*, vol. 44, no. 26, May 2011, Art. no. 265301, doi: 10.1088/1751-8113/44/26/265301.

[13] L. Luca and V. Romano, "Quantum corrected hydrodynamic models for charge transport in graphene," *Ann. Phys.*, vol. 406, pp. 30–53, Jul. 2019, doi: 10.1016/j.aop.2019.03.018.

[14] G. Mascali and V. Romano, "Charge transport in graphene including thermal effects," *SIAM J. Appl. Math.*, vol. 77, no. 2, pp. 593–613, Jan. 2017, doi: 10.1137/15M1052573.

[15] V. D. Camiola and V. Romano, "Hydrodynamical model for charge transport in graphene," *J. Stat. Phys.*, vol. 157, no. 6, pp. 1114–1137, Dec. 2014, doi: 10.1007/s10955-014-1102-z.

[16] L. Luca and V. Romano, "Comparing linear and nonlinear hydrodynamical models for charge transport in graphene based on the maximum entropy principle," *Int. J. Non-Linear Mech.*, vol. 104, pp. 39–58, Sep. 2018, doi: 10.1016/j.ijnonlinmec.2018.01.010.

[17] A. Majorana, G. Mascali, and V. Romano, "Charge transport and mobility in monolayer graphene," *J. Math. Ind.*, vol. 7, no. 1, Aug. 2016, Art. no. 4, doi: 10.1186/s13362-016-0027-3.

[18] G. Nastasi and V. Romano, "Improved mobility models for charge transport in graphene," *Commun. Appl. Ind. Math.*, vol. 10, no. 1, pp. 41–52, May 2019, doi: 10.1515/caim-2019-0011.

[19] P. Nemes-Incze, Z. Osváth, K. Kamarás, and L. P. Biró, "Anomalies in thickness measurements of graphene and few layer graphite crystals by tapping mode atomic force microscopy," *Carbon*, vol. 46, no. 11, pp. 1435–1442, Sep. 2008, doi: 10.1016/j.carbon.2008.06.022.

[20] C. J. Shearer, A. D. Slattery, A. J. Stapleton, J. G. Shapter, and C. T. Gibson, "Accurate thickness measurement of graphene," *Nanotechnology*, vol. 27, no. 12, Feb. 2016, Art. no. 125704, doi: 10.1088/0957-4484/27/12/125704.

[21] A. C. Ferrari *et al.*, "Science and technology roadmap for graphene, related two-dimensional crystals, and hybrid systems," *Nanoscale*, vol. 7, no. 11, pp. 4598–4810, Sep. 2015, doi: 10.1039/C4NR01600A.

[22] J. H. Chang, A. Huzayyin, K. Lian, and F. Dawson, "Quantum capacitance of graphene in contact with metal," *Appl. Phys. Lett.*, vol. 107, no. 19, Nov. 2015, Art. no. 193902, doi: 10.1063/1.4935365.

[23] J. G. Champlain, "A first principles theoretical examination of graphene-based field effect transistors," *J. Appl. Phys.*, vol. 109, no. 8, Apr. 2011, Art. no. 084515, doi: 10.1063/1.3573517.

[24] G. Nastasi and V. Romano, "A full coupled drift-diffusion-Poisson simulation of a GFET," *Commun. Nonlinear Sci. Numer. Simul.*, vol. 87, Aug. 2020, Art. no. 105300, doi: 10.1016/j.cnsns.2020.105300.

[25] M. G. Ancona, "Electron transport in graphene from a diffusion-drift perspective," *IEEE Trans. Electron Devices*, vol. 57, no. 3, pp. 681–689, Mar. 2010, doi: 10.1109/TED.2009.2038644.

[26] C. Jacoboni, "Semiconductors," in *Theory of Electron Transport in Semiconductors*, 1st ed. Berlin, Germany: Springer-Verlag, 2010, pp. 103–123.

[27] C. Kittel, "Semiconductor crystals," in *Introduction to Solid State Physics*, 7th ed. Hoboken, NJ, USA: Wiley, 2005, pp. 185–219.

[28] A. H. C. Neto, F. Guinea, N. M. R. Peres, K. S. Novoselov, and A. K. Geim, "The electronic properties of graphene," *Rev. Mod. Phys.*, vol. 81, no. 1, pp. 109–162, 2009, doi: 10.1103/RevModPhys.81.109.

[29] O. Frank, J. Vejpravova, V. Holy, L. Kavan, and M. Kalbac, "Interaction between graphene and copper substrate: The role of lattice orientation," *Carbon*, vol. 68, pp. 440–451, Mar. 2014, doi: 10.1016/j.carbon.2013.11.020.

[30] A. L. Walter *et al.*, "Electronic structure of graphene on single-crystal copper substrates," *Phys. Rev. B, Condens. Matter*, vol. 84, no. 19, Nov. 2011, Art. no. 195443, doi: 10.1103/PhysRevB.84.195443.

[31] F. Xia, V. Perebeinos, Y.-M. Lin, Y. Wu, and P. Avouris, "The origins and limits of metal–graphene junction resistance," *Nature Nanotechnol.*, vol. 6, no. 3, pp. 179–184, Mar. 2011, doi: 10.1038/NNANO.2011.6.

[32] P. C. Feijoo, D. Jiménez, and X. Cartoixà, "Short channel effects in graphene-based field effect transistors targeting radio-frequency applications," *2D Mater.*, vol. 3, no. 2, Jun. 2016, Art. no. 025036, doi: 10.1088/2053-1583/3/2/025036.